Tuning the magnetic coupling across ultrathin antiferromagnetic films by controlling atomic-scale roughness

W. KUCH[1,2]*, L. I. CHELARU[1], F. OFFI[1], J. WANG[1], M. KOTSUGI[1] AND J. KIRSCHNER[1]

[1]Max-Planck-Institut für Mikrostrukturphysik, Weinberg 2, D-06120 Halle, Germany
[2]Freie Universität Berlin, Institut für Experimentalphysik, Arnimallee 14, D-14195 Berlin, Germany
*e-mail: kuch@physik.fu-berlin.de

Published online: 8 January 2006; doi:10.1038/nmat1548

Characterization and control of the interface structure and morphology at the atomic level is an important issue in understanding the magnetic interaction between an antiferromagnetic material and an adjacent ferromagnet in detail, because the atomic spins in an antiferromagnet change direction on the length scale of nearest atomic distances. Despite its technological importance for the development of advanced magnetic data-storage devices and extensive studies, the details of the magnetic interface coupling between antiferromagnets and ferromagnets have remained concealed. Here we present the results of magneto-optical Kerr-effect measurements and layer-resolved spectro-microscopic magnetic domain imaging of single-crystalline ferromagnet–antiferromagnet–ferromagnet trilayers. Atomic-level control of the interface morphology is achieved by systematically varying the thicknesses of the bottom ferromagnetic and the antiferromagnetic layer. We find that the magnetic coupling across the interface is mediated by step edges of single-atom height, whereas atomically flat areas do not contribute.

Antiferromagnetic materials are widely used in magnetic thin-film devices, such as magnetic hard-disk read heads or sensors, and are also expected to play a principal role in future applications such as magnetic random-access memories[1] or magneto-logic devices[2,3]. The use of antiferromagnetic materials has also been proposed as a possible recipe to stabilize the magnetization of nanometre-sized particles at room temperature[4], an important prerequisite for pushing the density of magnetic information storage much beyond today's limits. Placing an antiferromagnetic material in contact with a ferromagnetic film modifies the magnetic switching behaviour of the latter, which is vital for the independent control of magnetization of the different magnetic layers making up a magnetoresistive element. In general, the magnetic field necessary for switching the magnetization is increased markedly by the interaction at the ferromagnet–antiferromagnet interface, and can induce a unidirectional anisotropy leading to a preferred magnetization direction of the ferromagnetic layer ('exchange bias')[5,6]. Although this effect is widely used in magnetoresistive devices, a detailed fundamental understanding of the magnetic interaction between antiferromagnet and ferromagnet is still elusive. This is, in part, because of the insufficient characterization of the interface structure in the polycrystalline materials that are typically used to study exchange bias. In antiferromagnetic materials the direction of the atomic magnetic moments varies on the lengthscale of atomic distances, leading to zero net magnetization if averaged over a few lattice constants. Atomic-scale control and characterization of the antiferromagnetic–ferromagnetic interface is thus essential for a fundamental understanding of the magnetic interaction between antiferromagnetic and ferromagnetic materials. The presence of interface roughness is indeed a necessary ingredient in some models of exchange bias[6,7].

We studied the magnetic interface coupling between antiferromagnetic and ferromagnetic films at well-defined single-crystalline interfaces, in which we can controllably vary the number of monatomic steps at the otherwise atomically flat interfaces. Ultrathin single-crystalline antiferromagnetic FeMn films can be

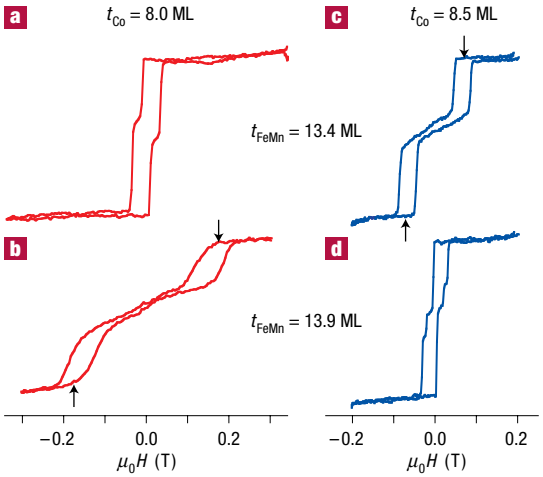

Figure 1 Effect of the thickness of the antiferromagnetic FeMn layer t_{FeMn} and the bottom ferromagnetic Co layer t_{Co} on the magnetization loops of single-crystalline Co–FeMn–Co trilayers, deposited on Cu(001). The thickness of the top Co layer was 6 ML in all cases. The loops were measured by *in situ* magneto-optical Kerr effect. **a**, Magnetization loop for $t_{FeMn} = 13.4$ ML, $t_{Co} = 8.0$ ML showing ferromagnetic interlayer coupling between the two Co layers. **b**, Magnetization loop for $t_{FeMn} = 13.9$ ML, $t_{Co} = 8.0$ ML showing antiferromagnetic coupling between the two Co layers. **c**,**d**, Magnetization loops at the same FeMn thicknesses but for $t_{Co} = 8.5$ ML. At that Co thickness the sample with $t_{FeMn} = 13.4$ ML has antiparallel coupling (**c**), whereas the sample with $t_{FeMn} = 13.9$ ML shows parallel coupling (**d**). The arrows indicate the saturation field used for estimating the antiferromagnetic coupling strength. The FeMn layer was deposited as a wedge in which the thickness varied by 1.5 ML over 6 mm by moving a shutter in front of the sample during deposition of 1.5 ML FeMn on top of a 13.8 ML continuous FeMn film.

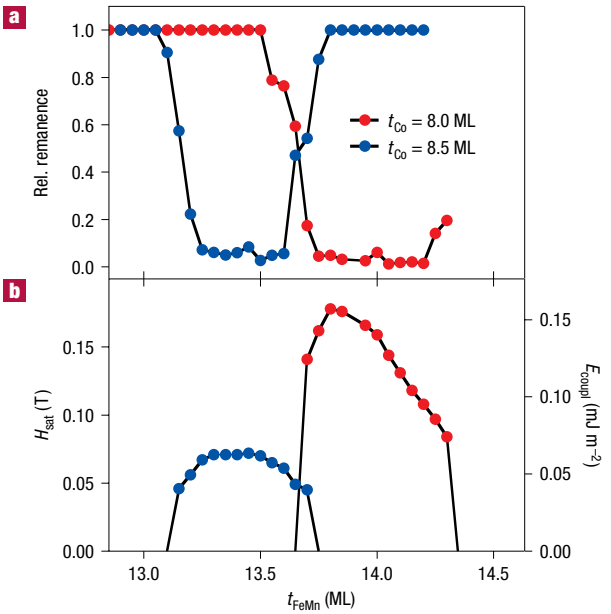

Figure 2 Influence of the atomic layer filling of the bottom Co layer on the position and the strength of the antiferromagnetic interlayer coupling maximum across a single-crystalline antiferromagnetic FeMn layer in Co–FeMn–Co trilayers on Cu(001). a, Remanence-to-saturation ratio of magnetization loops measured by magneto-optical Kerr effect as a function of the thickness of the FeMn layer for integer layer filling of the bottom Co layer ($t_{Co} = 8.0$ ML, red) and for half-integer filling ($t_{Co} = 8.5$ ML, blue). The position of the FeMn thickness range for antiparallel interlayer coupling is shifted significantly between the two cases. **b**, Corresponding saturation field (left axis) and estimated interlayer coupling energy (right axis) for the antiparallel interlayer coupling across FeMn as a function of the thickness of the FeMn layer.

grown on Cu(001) single-crystal surfaces owing to the low lattice misfit (≈0.4%; ref. 8). Deposition at room temperature leads to epitaxial growth of FeMn in a layer-by-layer fashion, in which atomic layers are filled successively by nucleation and subsequent expansion of one-atom-high FeMn islands[9]. This layer-by-layer growth is continued if a ferromagnetic Co film is deposited on top of an FeMn film, or if FeMn is grown on top of a Co film[8], whereas partly filled atomic surface layers are completed by atoms of the next film[10]. The face-centred-cubic (f.c.c.) FeMn films have a three-dimensional non-collinear antiferromagnetic spin structure[11] with magnetically compensated (001) crystallographic planes, and show a moderate exchange bias effect at thicknesses above about 20 atomic monolayers (ML); ref. 8.

The magnetic interlayer coupling in trilayers of the type ferromagnet–FeMn–Co, where Co or FeNi was used as the top ferromagnetic layer, was investigated as a measure of the strength of the antiferromagnetic–ferromagnetic coupling at the two interfaces. By varying the thickness of the bottom Co layer by less than 1 ML, the atomic-scale morphology of the interface to the antiferromagnetic FeMn layer can be modified, and the role of atomic steps, islands and vacancy islands at the interface for the magnetic interaction between antiferromagnetic and ferromagnetic layers can be studied. We find that the antiferromagnetic–ferromagnetic coupling depends strongly on the atomic layer filling at the interface, and varies by more than a factor of two between filled and half-filled interface layers. Furthermore, we observe a pronounced systematic dependence of the antiferromagnetic layer thickness for maximum interlayer coupling strength on the atomic-scale interface morphology, which shows that islands and vacancy islands at the interface lead to a quite distinct coupling behaviour. Our experimental results thus demonstrate the importance not only of the presence of atomic steps at the interface, but also their detailed arrangement.

Magnetization loops of Co–FeMn–Co trilayers reveal the magnetic coupling across the FeMn antiferromagnetic layer for different thicknesses of the Co bottom layer and the FeMn antiferromagnetic layer (Fig. 1). The thickness of the top Co layer was kept constant at 6 ML for all four loops shown in Fig. 1. The magnetization loops for a thickness of the bottom Co layer t_{Co} of 8.0 ML are shown in Fig. 1a and b. The roughness of the interface with the FeMn layer has a local minimum at that integer atomic-layer thickness. Measurements at two representative FeMn-layer thicknesses t_{FeMn} of 13.4 and 13.9 ML have quite different loops: Fig. 1a for $t_{FeMn} = 13.4$ ML shows an almost square shape with a remanence equal to saturation. Both Co layers are thus magnetized in parallel at zero field. On the other hand, Fig. 1b for $t_{FeMn} = 13.9$ ML has a loop typical for antiparallel coupling between the two Co layers. Here the remanence at zero field is close to zero, corresponding to an antiparallel alignment of the two Co layers. As will be shown below, the coupling between the two ferromagnetic layers oscillates from parallel to antiparallel with a period of 2 ML of t_{FeMn}. This is expected if the interlayer coupling is mediated by the antiparallel nearest-neighbour exchange interaction in the antiferromagnetic layer, which transfers any local modification of the spin structure at one interface to the other with a period of 2 ML (ref. 12).

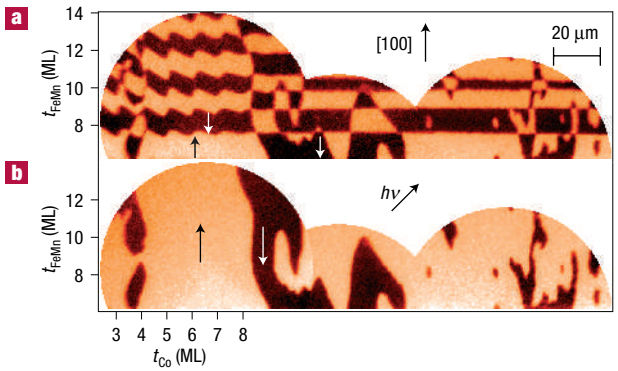

Figure 3 Overview of the direction of the magnetic interlayer coupling in an FeNi–FeMn–Co single-crystalline trilayer on Cu(001). The bottom Co layer and antiferromagnetic FeMn layer were deposited as crossed wedges with thicknesses indicated at the bottom and left axes, respectively. The Co thickness increases from left to right up to 8 ML, and then stays constant at 8 ML. The thickness of the top FeNi layer is 6 ML. Layer-resolved magnetic domain images of the as-grown trilayer are presented, acquired by XMCD-PEEM at the Fe and Co L_3 absorption edges. **a**, Layer-resolved domain image of the top FeNi layer. **b**, Layer-resolved domain image of the bottom Co layer. Arrows labelled [100] and $h\nu$ show the crystallographic orientation of the substrate and the direction of X-ray incidence, arrows inside the domain images indicate local magnetization directions. From comparison of the two domain images, regions of parallel and antiparallel coupling in the two-dimensional thickness space can be deduced. In addition to an oscillating coupling as a function of FeMn thickness, a periodic shift of this oscillation as a function of Co thickness in the region of the Co wedge is also observed as a sawtooth-like wiggle of the horizontal stripes in **a**.

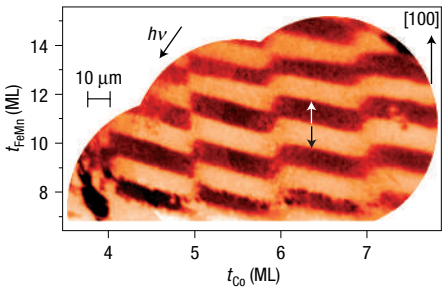

Figure 4 Overview of the direction of the magnetic interlayer coupling in Co–Ni–FeMn–Co on Cu(001). The bottom Co layer and antiferromagnetic FeMn layer were deposited as crossed wedges with thicknesses indicated at the bottom and left axes, respectively. The top ferromagnetic layer consisted of 3 ML Co/15 ML Ni. The image has been acquired at the Ni L_3 absorption edge, representing the layer-resolved domain image of the top ferromagnetic layer. As in Fig. 3, an oscillation of the coupling direction as a function of FeMn thickness and a pronounced, sawtooth-like modulation of the phase of that oscillation as a function of the Co bottom layer atomic filling is evident.

Surprisingly the magnetization loops change quite markedly on adding 0.5 ML ferromagnetic material in the bottom layer (Fig. 1c,d). The graphs in Fig. 1c and d show loops for the same FeMn thicknesses as Fig. 1a and b. The only difference here is that the thickness of the bottom Co layer was now 8.5 instead of 8.0 ML. The roughness of the bottom interface has a local maximum at that half-integer atomic Co layer thickness. Now the loop observed for 13.9 ML FeMn thickness (Fig. 1d) is almost square, whereas at $t_{FeMn} = 13.4$ ML antiparallel coupling across the FeMn layer is observed (Fig. 1c).

A compilation of the remanence-to-saturation ratio as a function of t_{FeMn} of all loops measured for $t_{Co} = 8.0$ and 8.5 ML (Fig. 2a) clearly shows the change in the FeMn thickness for antiparallel coupling induced exclusively by the atomic-scale roughness of the Co–FeMn interface. Values close to zero correspond to antiparallel coupling between the two Co layers, values of one indicate parallel or weak coupling. A significant shift of the region of antiparallel coupling towards lower FeMn thicknesses on increasing the bottom Co–FeMn interface roughness is evident. Not only the FeMn thickness at which antiparallel coupling occurs, but also the strength of that coupling depend strongly on the Co bottom layer thickness, that is, on the roughness of the bottom Co–FeMn interface. A measure for the coupling strength in the case of antiparallel interlayer coupling is the magnetic field needed to align the two ferromagnetic layer magnetizations in parallel, the saturation field H_{sat}. We used the field at the centre of the minor hysteresis loop on each side of the magnetization curve, as indicated in Fig. 1b and c by small black arrows. The dependence of H_{sat} on t_{FeMn} is plotted in Fig. 2b. The highest H_{sat} needed for $t_{Co} = 8.0$ ML is about 2.5 times higher than in the case of $t_{Co} = 8.5$ ML. A rough estimate of the coupling energy E_{coupl} can be obtained from H_{sat} using $E_{coupl} = M_{S,Co} H_{sat} (1/t_1 + 1/t_2)^{-1}$, if one neglects the influence of magnetic anisotropy on H_{sat}. Here t_1 and t_2 are the thicknesses of the two Co layers, and $M_{S,Co}$ is the Co saturation magnetization. Values for E_{coupl} using $t_1 = 1.5$ nm, $t_2 = 1.1$ nm and $M_{S,Co} = 1{,}440$ kA m^{-1} are shown on the right axis of Fig. 2b.

A more complete view of the thickness dependence of the interlayer coupling on both the Co bottom layer thickness and the FeMn antiferromagnetic layer thickness is obtained from layer-resolved magnetic-imaging experiments, performed on crossed double-wedge samples. Figure 3 shows layer-resolved magnetic domain images of a NiFe–FeMn–Co trilayer on Cu(001), in which the Co bottom ferromagnetic layer and the FeMn antiferromagnetic layer have been deposited as crossed micro-wedges suitable for photoelectron emission microscopy (PEEM) imaging[13]. NiFe was used as the top ferromagnetic layer here to image the magnetic domain pattern of the top and bottom ferromagnetic layer separately, taking advantage of the element-selectivity of X-ray magnetic circular dichroism (XMCD). In Fig. 1a the as-grown domain image of the top FeNi layer is shown, whereas Fig. 1b shows the domain image of the bottom Co layer, as seen through the FeNi and FeMn overlayers. The Co layer thickness increases up to 8 ML from left to right as indicated on the bottom axis of Fig. 3, and then remains constant at 8 ML. The FeMn thickness increases in the field of view from 6 to 14 ML from bottom to top, as indicated on the left axis. We observe antiferromagnetism at room temperature in that trilayer for FeMn thicknesses above 6 ML, as exhibited by a 45° change of Co magnetization direction[14,15]. Dark and bright regions in Fig. 3 correspond to domains with magnetization in the plane pointing up and down along the [100] and [$\bar{1}$00] crystallographic directions, as indicated by arrows. From the comparison of the two domain images, regions in two-dimensional Co and FeMn thickness space with parallel and antiparallel coupling between the two ferromagnetic layers can be immediately recognized as horizontal stripes in Fig. 3a. They appear periodically as a function of FeMn thickness, with a period of 2 ML. The influence of the Co bottom layer thickness is recognized as a further sawtooth-like corrugation of the stripes in the left part of the image, in the region where the Co thickness increases. It is a periodic function of Co thickness with a period of 1 ML. This clearly shows that it is related to the morphology of the Co–FeMn interface during the layer-by-layer growth. Another example is presented in Fig. 4.

Here the bottom part of the sample was again an FeMn–Co crossed wedge with thicknesses indicated on the left and bottom axes, and the top ferromagnetic layer consisted of 3 ML Co on top of 15 ML Ni. In Fig. 4 the contrast at the Ni L_3 edge is shown, representing the domain pattern of the top layer. Although all the samples were grown with no external magnetic field applied, the bottom ferromagnetic layer showed a uniform white contrast in the region of the image, corresponding to magnetization along [$\bar{1}$00]. Bright and dark stripes in Fig. 4 indicate parallel and antiparallel alignment of the top and bottom ferromagnetic layer magnetizations, respectively. The two main features, a periodic oscillatory interlayer coupling across the FeMn layer with a period of 2 ML in FeMn thickness and a periodic modulation of the phase of this coupling as a function of Co bottom layer thickness with a period of 1 ML, are again immediately recognized.

The shape of the modulation of the coupling phase is clearly different from a sinusoidal behaviour. On increasing the Co thickness, sudden jumps of the coupling phase occur at about integer atomic layer fillings, followed by a linear decrease of the phase. It is therefore not only the interface roughness that matters for the coupling. The interface roughness during layer-by-layer growth has maxima at around 50% atomic layer fillings and decreases towards both sides, for higher and lower fillings, leading to the sine-like oscillations typically observed in the diffracted electron intensity[8]. In the present case, however, a 20% filling of the Co interface atomic layer, for example, is completely different from an 80% filling, although the number of monatomic steps and thus the roughness may be equal. Our model that accounts for such a sawtooth-like behaviour is explained in Fig. 5a,b. The observed shift of the coupling phase can be obtained by assuming that not all the FeMn deposited (denoted by the nominal antiferromagnetic layer thickness t_{AF}) mediates the coupling, but only a part (denoted by the effective antiferromagnetic layer thickness $t_{AF,eff}$), $t_{AF,eff} \leq t_{AF}$. In fact a sawtooth-like shift as observed in the experiment would arise if only complete FeMn atomic layers contributed to the coupling. The difference between $t_{AF,eff}$ and t_{AF} corresponds to the FeMn in mixed Co–FeMn atomic layers at the interfaces and leads to the sawtooth-like behaviour.

We can now draw several conclusions:

(i) As in Fig. 2 the maximum for antiparallel coupling occurs at higher FeMn thickness for 8.0 ML Co bottom layer thickness and the sawtooth-like modulation is less than 1 ML, the upwards jump as sketched in Fig. 5 must have happened at a Co thickness just below 8.0 ML. This is reasonable, as during the layer-by-layer growth of Co on Cu(001) islands of the next atomic layer are already formed somewhat before completion of the previous layer[16].

(ii) The regions of antiparallel coupling shown in Fig. 2 have to correspond to 12 complete (Co-free) FeMn layers, as an even number of complete antiferromagnetic atomic layers should lead to antiparallel coupling. This means that, in both cases, top-layer Co islands are no longer present in the 12th complete FeMn layer or, in other words, that vacancy islands reaching down to the 11th layer disappear at $13.2 - 0.5 = 12.7$ ML or at $13.7 - 1.0 = 12.7$ ML in the two cases. This is reasonable if one considers that at the upper interface the layer-by-layer growth is probably less perfect than at the bottom interface. In other words, in the case of 8.0 ML (8.5 ML) Co bottom layer, about 1 ML (0.5 ML) FeMn is filling the 9th Co layer, and between 0.7 and 1.3 ML FeMn form islands on top of the FeMn film, so that the number of complete FeMn atomic planes is 12 for total thicknesses between about 13.7 and 14.3 ML (13.2 and 13.8 ML).

(iii) The coupling strength across the FeMn layer is clearly higher for 8.0 ML Co thickness. In this case we are dealing with a quite smooth bottom interface with only small islands of the 9th layer[17]. In the case of 8.5 ML Co bottom layer thickness, the interface consists of monatomic grooves and islands, each making up 50% of the area[16]. As the coupling sign is dictated by the height of the islands, smaller islands mediate a stronger interlayer coupling even though they may cover much less of the surface.

(iv) The coupling strength estimated in both cases is much lower than what would be expected for a direct exchange coupling through the entire antiferromagnetic spacer layer. From the bulk Néel temperature of $Fe_{50}Mn_{50}$ (500 K; ref. 18), one can estimate[19] the exchange constant A inside the FeMn layer as about 3×10^{-12} J m^{-1} (ref. 20). In the simplest case, neglecting any anisotropy of the antiferromagnetic layer, the energy needed to turn the spin direction of one of the antiferromagnetic interfaces by creating a twisted helical spin structure inside a layer of thickness d is given by $\pi^2 A/d$, which for $d = 2.5$ nm is more than 10 mJ m^{-2},

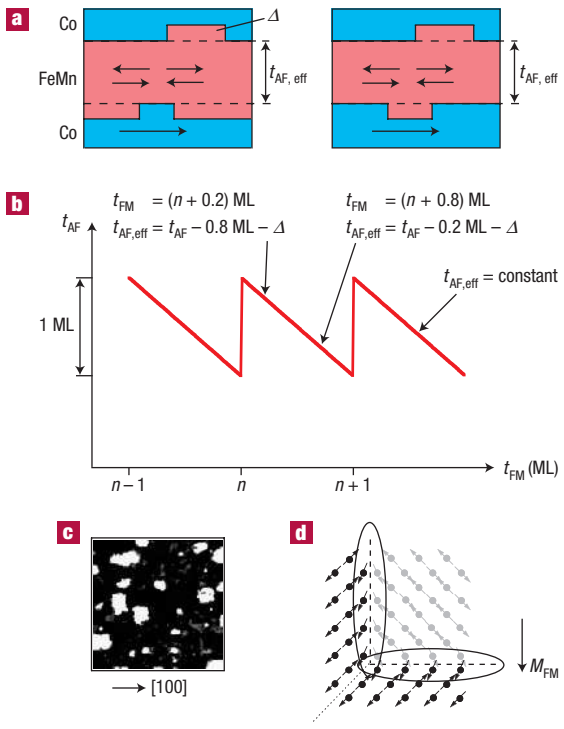

Figure 5 Schematic explanation of the model used to explain the observed sawtooth-like behaviour of the sign of the magnetic interlayer coupling across single-crystalline antiferromagnetic FeMn layers. a, Sketch showing the dependence of the effective antiferromagnetic layer thickness $t_{AF,eff}$ on the interface layer filling of the bottom ferromagnetic layer: if the filling is 0.2 ML, then the deposited amount of FeMn (t_{AF}) and $t_{AF,eff}$ differ by 0.8 ML plus an amount Δ filling the interface to the top Co layer (left); if it is 0.8 ML, they differ by 0.2 ML plus Δ (right). **b**, Two-dimensional plot of the bottom ferromagnetic layer thickness t_{FM} and t_{AF}, in which a line of constant $t_{AF,eff}$ shows a sawtooth-like behaviour as experimentally observed. Such a line could be, for example, the transition line between parallel and antiparallel coupling. **c**, Scanning tunnelling microscopy image (50×50 nm^2) of the surface of 9.15 ML FeMn on Cu(001). Black and white areas mark the 9th and 10th atomic layer, respectively. **d**, Sketch of a possible interface spin configuration of the antiferromagnetic layer in a 3Q spin structure[11] at step edges running along ⟨100⟩ crystallographic directions. Grey and black arrows indicate the in-plane direction of spins of next-level atomic planes. Ellipses at the step edges (dashed lines) indicate regions in which antiferromagnetic spins do not cancel, but follow the magnetization direction M_{FM} of the ferromagnetic layer. Here, the direction of these spins may be twisted. Antiphase domain boundaries in the antiferromagnetic layer (dotted line) may occur to adapt the uncompensated antiferromagnetic spins to the magnetization direction of the ferromagnet.

about two orders of magnitude higher than the experimentally observed energy needed to break the maximum antiferromagnetic coupling across the antiferromagnetic FeMn layer.
(v) The antiferromagnetic material filling the last incomplete atomic layer of the bottom ferromagnetic film and 'missing' for the interlayer coupling cannot be simply ferromagnetic and aligned with the ferromagnetic layer magnetization, as no oscillatory behaviour of the induced net magnetic moment in Fe and Mn has been observed[10]. Furthermore, the estimated amount of induced uncompensated Fe moments aligned ferromagnetically with the Co from these studies was constant and made up only about 30% of the Fe of one interfacial atomic layer.
(vi) Interestingly, competition between parallel and antiparallel magnetic interlayer coupling on a lengthscale smaller than the typical magnetic lengthscale is not present in this system. Such competition would lead to the occurrence of 90° coupling[21–23]. No sign of 90° coupling of the two ferromagnetic layers across the single-crystalline FeMn layers is observed.

There are some interesting consequences. The coupling between ferromagnetic and antiferromagnetic layers is mediated mainly by uncompensated spins of the antiferromagnetic layer at monoatomic step edges at the interface. A possible configuration is sketched in Fig. 5d. Flat terraces do not contribute significantly to the antiferromagnetic–ferromagnetic coupling, as this would lead to a non-collinear or 90° coupling. The observed coupling strength is indeed consistent with a contribution of about 1–2% of the interface area. This is compatible with an antiferromagnetic spin structure in which the interface atom spins of atomically flat terraces cancel out[11].

The coupling is stronger if the steps are confined at small islands (Fig. 5c), and partly averages out if islands become larger. The probability of having uncompensated spins at the step edges of an island decreases if the island size is increased because in that case the chance for uncompensated edge atom spins to cancel out is increasing. This is in line with Malozemoff's model of exchange bias[7], and the observed inverse dependence of exchange bias on interfacial grain size in polycrystalline films[24] and on domain size[25].

The interlayer coupling must be transferred through the antiferromagnetic layer by a uniaxial modification of the antiferromagnetic spin structure, which, because of the antiferromagnetic exchange interaction inside the antiferromagnetic layer, leads to an oscillation of the direction of the coupling with a period of two atomic layers. Note that owing to the random orientation of step edges leading to uncompensated spins of the antiferromagnetic layer, its spin structure will have many small domains when grown on top of a ferromagnetic layer (Fig. 5d). This is because of the same mechanism that breaks a ferromagnetic layer into small domains when the antiferromagnetic layer is deposited first[14,15].

Although the results presented here are specific for single-crystalline antiferromagnetic FeMn films, they also contain more general important aspects. Light is shed, for the first time, on the detailed coupling mechanism between an antiferromagnetic layer and adjacent ferromagnetic layers. Our results indicate that, in general, the interface coupling of systems with compensated antiferromagnetic interface spin structure can be enhanced by the controlled incorporation of atomic-level roughness features with small lateral size. With the forthcoming advent of atomic-scale manipulation in nanotechnology, this may be a feasible way to controllably modify the coupling strength in ferromagnetic–antiferromagnetic systems. Coupling of ferromagnetic nanoparticles to an antiferromagnetic layer may also have important consequences for attempts to overcome the superparamagnetic limit by the use of antiferromagnetic materials[4]. It has to be verified whether magnetic nanoparticles in a dense array of particles supported on an antiferromagnetic layer are magnetically independent, and that the observed increase in blocking temperature is not the consequence of magnetic coupling between particles. The influence of the antiferromagnet on the anisotropy of the particles may then be tailored by nanosculpting the interface to achieve the desired high blocking temperature.

METHODS

Films were grown by molecular beam epitaxy on a Cu(001) single-crystal surface kept at room temperature, using commercially available evaporation sources (Omicron). FeNi and FeMn layers were deposited by co-evaporation from two different sources. All experiments were carried out *in situ* in the same ultrahigh vacuum chamber in which the films were deposited (base pressure 1×10^{-10} mbar). Film thicknesses were monitored with 0.1 atomic ML accuracy by intensity oscillations in the specularly reflected electron intensity during deposition.

Magnetization loops were obtained by *in situ* longitudinal magneto-optical Kerr effect. *s*-polarized light from a laser diode, operated at a wavelength of 675 nm, was obtained by a polarizer and focused on the sample by an optical lens. The angle of incidence was about 70° from the surface normal. The sample rested in a glass finger connected to the ultrahigh vacuum chamber reaching into the core gap of an electromagnet, in which the field was applied in the plane of the sample in the direction of the laser light. The reflected light passed through a 50 kHz photoelastic modulator and an analysing polarizer before reaching a photodiode detector. The signal was obtained using a lock-in amplifier with the reference signal from the modulator. A linear background caused by the Faraday effect of the optical lens was subtracted.

XMCD PEEM with synchrotron radiation was used for the element-resolved magnetic domain imaging[26]. In this technique, the dependence of absorption of circularly polarized X-rays at elemental absorption resonances on the direction of magnetization is mapped by the intensity of emitted secondary electrons[27,28]. Experiments were performed at beamline UE56/2-PGM2 of BESSY in Berlin using a commercially available PEEM (Focus IS-PEEM), described in more detail in ref. 29. The angle of incidence of the X-rays was 60° from the surface normal. The wavelength of the exciting radiation was tuned to the maxima of the L_3 absorption edges of Fe, Co or Ni to obtain the element-resolved magnetic contrast.

Received 11 March 2005; accepted 28 October 2005; published 8 January 2006.

References

1. Parkin, S. S. P. *et al.* Exchange-biased magnetic tunnel junctions and application to nonvolatile magnetic random access memory. *J. Appl. Phys.* **85,** 5828–5833 (1999).
2. Prinz, G. A. Device physics—magnetoelectronics. *Science* **282,** 1660–1663 (1998).
3. Wolf, S. A. *et al.* Spintronics: A spin-based electronics vision for the future. *Science* **294,** 1488–1495 (2001).
4. Skrumryev, V. *et al.* Beating the superparamagnetic limit with exchange bias. *Nature* **423,** 850–853 (2003).
5. Nogués, J. & Schuller, I. K. Exchange bias. *J. Magn. Magn. Mater.* **192,** 203–232 (1999).
6. Stamps, R. L. Mechanisms for exchange bias. *J. Phys. D* **33,** R247–R268 (2000).
7. Malozemoff, A. P. Random-field model of exchange anisotropy at rough ferromagnetic-antiferromagnetic interfaces. *Phys. Rev. B* **35,** 3679–3682 (1987).
8. Offi, F., Kuch, W. & Kirschner, J. Structural and magnetic properties of Fe_xMn_{1-x} thin films on Cu(001) and on Co/Cu(001). *Phys. Rev. B* **66,** 064419 (2002).
9. Kuch, W., Chelaru, L. I. & Kirschner, J. Surface morphology of antiferromagnetic $Fe_{50}Mn_{50}$ layers on Cu(001). *Surf. Sci.* **566–568,** 221–225 (2004).
10. Offi, F. *et al.* Induced Fe and Mn magnetic moments in Co-FeMn bilayers on Cu(001). *Phys. Rev. B* **67,** 094419 (2003).
11. Kuch, W. *et al.* Three-dimensional noncollinear antiferromagnetic order in single-crystalline FeMn ultrathin films. *Phys. Rev. Lett.* **92,** 017201 (2004).
12. Liu, Z. Y. & Adenwalla, S. Oscillatory interlayer exchange coupling and its temperature dependence in $[Pt/Co]_3$/NiO/$[Co/Pt]_3$ multilayers with perpendicular anisotropy. *Phys. Rev. Lett.* **91,** 037207 (2003).
13. Kuch, W. *et al.* Imaging microspectroscopy of Ni/Fe/Co/Cu(001) using a photoemission microscope. *J. Electron Spectrosc. Relat. Phenom.* **109,** 249–265 (2000).
14. Kuch, W. *et al.* Magnetic interface coupling in single-crystalline Co/FeMn bilayers. *Phys. Rev. B* **65,** 140408 (2002).
15. Won, C. *et al.* Studies of FeMn/Co/Cu(001) films using photoemission electron microscopy and surface magneto-optic Kerr effect. *Phys. Rev. B* **71,** 024406 (2005).
16. Schmid, A. K. & Kirschner, J. In situ observation of epitaxial growth of Co thin films on Cu(100). *Ultramicroscopy* **42–44,** 483–489 (1992).
17. Schmid, A. K. *et al.* Fast interdiffusion in thin films: Scanning-tunneling-microscopy determination of surface diffusion through microscopic pinholes. *Phys. Rev. B* **48,** 2855–2858 (1993).
18. Umebayashi, H. & Ishikawa, Y. Antiferromagnetism of γ Fe-Mn alloys. *J. Phys. Soc. Jpn* **21,** 1281–1294 (1966).
19. Chikazumi, S. *Physics of Ferromagnetism* (Oxford Univ. Press, Oxford, 1997).
20. Sort, J. *et al.* Perpendicular exchange bias in antiferromagnetic–ferromagnetic nanostructures. *Appl. Phys. Lett.* **84,** 3696–3698 (2004).
21. Slonczewski, J. C. Fluctuation mechanism for biquadratic exchange coupling in magnetic multilayers. *Phys. Rev. Lett.* **67,** 3172–3175 (1991).

22. Slonczewski, J. C. Overview of interlayer exchange theory. *J. Magn. Magn. Mater.* **150,** 13–24 (1995).
23. Morosov, A. I. & Sigov, A. S. New type of domain walls: Domain wall caused by frustrations in multilayer magnetic nanostructures. *Phys. Solid State* **46,** 395–410 (2004).
24. Takano, K., Kodama, R. H., Berkowitz, A. E., Cao, W. & Thomas, G. Interfacial uncompensated antiferromagnetic spins: Role in unidirectional anisotropy in polycrystalline $Ni_{81}Fe_{19}$/CoO bilayers. *Phys. Rev. Lett.* **79,** 1130–1133 (1997).
25. Scholl, A. *et al.* Domain-size-dependent exchange bias in Co/$LaFeO_3$. *Appl. Phys. Lett.* **85,** 4085–4087 (2004).
26. Kuch, W. Layer-resolved microscopy of magnetic domains in multi-layered systems. *Appl. Phys. A* **76,** 665–671 (2003).
27. Stöhr, J. *et al.* Element-specific magnetic microscopy with circularly polarized x-rays. *Science* **259,** 658–661 (1993).
28. Schneider, C. M. & Schönhense, G. Investigating surface magnetism by means of photoexcitation electron emission microscopy. *Rep. Prog. Phys.* **65,** R1785–R1839 (2002).
29. Kuch, W., Chelaru, L. I., Offi, F., Kotsugi, M. & Kirschner, J. Magnetic dichroisms in absorption and photoemission for magnetic characterization in x-ray photoelectron emission microscopy. *J. Vac. Sci. Technol. B* **20,** 2543–2549 (2002).

Acknowledgements

This work was supported by the German Minister of Science and Education (BMBF) under grant no. 05 KS1EFA6. We thank B. Heinrich, J. T. Kohlhepp, and M. D. Stiles for fruitful discussions. Correspondence and requests for materials should be addressed to W.K.

Competing financial interests

The authors declare that they have no competing financial interests.